

<https://doi.org/10.1038/s42004-024-01377-y>

High triplet energy host material with a 1,3,5-oxadiazine core from a one-step interrupted Fischer indolization



Charlotte Riley¹, Hwan-Hee Cho², Alexander C. Brannan¹, Nguyen Le Phuoc³, Mikko Linnolahti³, Neil C. Greenham² & Alexander S. Romanov¹

Energy-efficient and deep-blue organic light-emitting diode (OLED) with long operating stability remains a key challenge to enable a disruptive change in OLED display and lighting technology. Part of the challenge is associated with a very narrow choice of the robust host materials having over 3 eV triplet energy level to facilitate efficient deep-blue emission and deliver excellent performance in the OLED device. Here we show the molecular design of new 1,3,5-oxadiazines (NON)-host materials with high triplet energy over 3.2 eV, enabling deep-blue OLED devices with a peak external quantum efficiency of 21%. A series of NON-host materials are prepared by the condensation of substituted arylhydrazines and cyclohexylcarbaldehyde in a 2:3 ratio. This straightforward “one-pot” procedure enables the formation of indoline-containing derivatives with three fused heterocyclic rings and two stereogenic centres. All materials emit UV-fluorescence in the range of 315–338 nm while possessing highly desirable characteristics for application in deep-blue OLED devices: good thermal stability, a wide energy gap (3.9 eV), a high triplet energy level of (3.3 eV), and excellent volatility during sublimation.

Since the seminal publication by Tang and Van Slyke in 1987, Organic Light-Emitting Diodes (OLEDs) have emerged as a dominant technology within the display and lighting industries¹. Significant progress in the OLED field has been driven by the development of new energy-efficient materials and OLED fabrication architectures². The first generation of OLED devices utilized organic fluorescent emitters. When charge is injected into an OLED device, it results in the simultaneous generation of one singlet and three triplet excitons, as determined by spin statistics. However, fluorescent emitters limit the internal quantum efficiency (IQE) of first-generation OLEDs to 25% due to nonradiative loss of the triplet excitons³. In contrast, the second and third generations of OLED devices achieve up to 100% IQE by harvesting all singlet and triplet excitons. This improvement is achieved through phosphorescence and thermally activated delayed fluorescence (TADF) mechanisms^{4–10}.

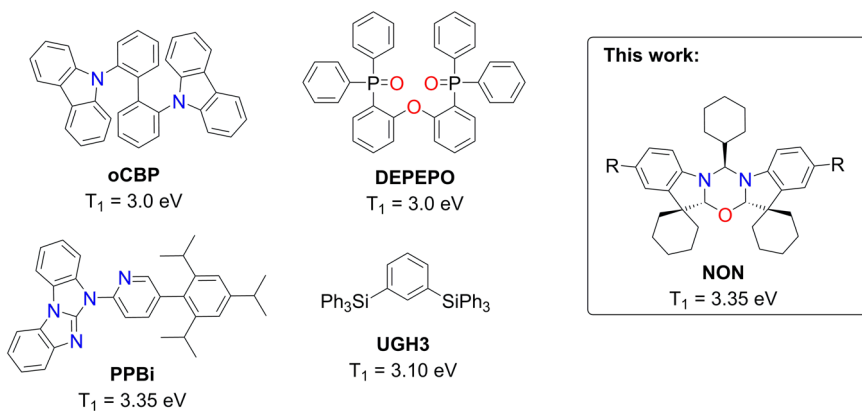
A significant challenge in the OLED field lies in developing energy-efficient blue OLEDs with high operating stability¹¹. Phosphorescent and TADF emitters often suffer from self-quenching due to triplet–triplet or triplet–polaron annihilation processes^{12,13}. To mitigate this, the “solid-state dilution” approach is employed, necessitating the use of a host matrix^{12,13}. Similar to emitter molecules, host materials must meet several criteria to enable energy-efficient and stable blue OLEDs. These include (1) a higher triplet (T_1) energy level compared with the emitter molecules to prevent

Dexter energy transfer to the host; (2) the highest occupied (HOMO) and lowest unoccupied (LUMO) molecular orbital energy levels for the host should confine those of the emitter molecule; (3) balanced charge-carrier (electron and hole) injection and mobility within the host; (4) high thermal and redox stability; (5) high volatility during the deposition process; (6) ability to enable slow roll-off of efficiency at high luminance, and many more¹⁴. All these requirements pose a unique challenge for blue OLED hosts, limiting the number of appropriate materials. Scheme 1 presents some of the most frequently used high triplet energy materials, illustrating various molecular design strategies used to achieve the necessary energetic properties for the blue OLED host materials^{15–17}. Synthetic protocols to obtain such hosts (Scheme 1) are optimized but involve expensive reagents and lengthy multistep syntheses which frequently employ transition metal catalysts that contribute to the final material cost. Additionally, the environmental impact of producing advanced materials (Scheme 1) is increased by necessary purification steps, such as a double sublimation¹⁸. In this work, we introduce a novel molecular design for a blue host material containing a 1,3,5-oxadiazine core which is unprecedented in the literature. Such NON-type materials are synthesised in a simple ‘one-pot’ reaction using inexpensive reagents in a good yield. We demonstrate that this new NON-type (Scheme 1) host material is compatible with deep-blue emitters. An external

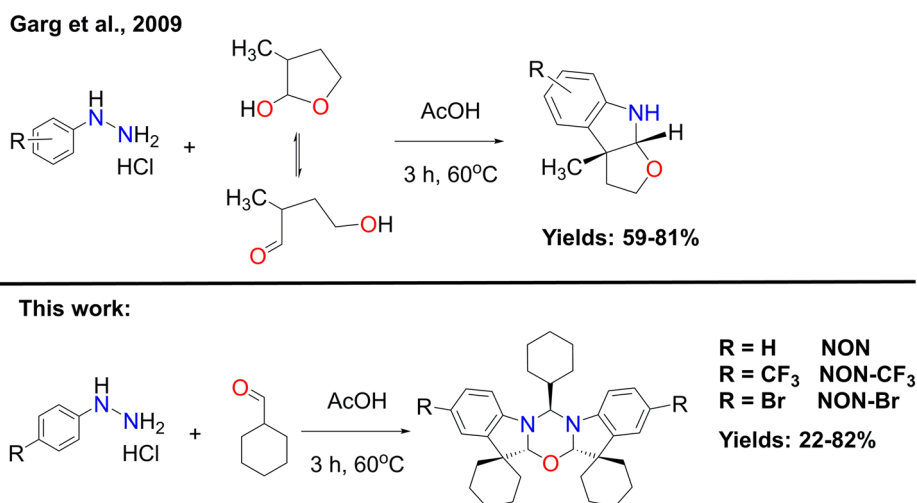
¹Department of Chemistry, The University of Manchester, Manchester, UK. ²Department of Physics, Cavendish Laboratory, Cambridge University, Cambridge, UK.

³Department of Chemistry, University of Eastern Finland, Joensuu, Finland. ✉ e-mail: mikko.linnolahti@uef.fi; ncg11@cam.ac.uk; alexander.romanov@manchester.ac.uk

Scheme 1 | Molecular structures for organic host materials. Molecular structure for popular DPEPO¹⁹, PPBi²⁰, UGH3⁴², oCBP^{29,43} and NON (R = H, CF₃ or Br) OLED host materials with triplet energy level more than 3.0 eV.



Scheme 2 | Synthetic protocols. One-step synthesis of the compounds NON, NON-CF₃ and NON-Br.



quantum efficiency (EQE) up to 21% was achieved in OLEDs with a device performance on par with hosts of complex molecular design, such as DPEPO¹⁹ or PPBi²⁰.

Results and discussion

Synthesis and characterization of NON-materials

The novel 1,3,5-oxadiazine compounds NON, NON-CF₃ and NON-Br were synthesized in one step by heating the substituted arylhydrazine hydrochlorides and cyclohexylcarbaldehyde in glacial acetic acid at 60 °C for 3 h (Scheme 2). The reaction forms three heterocyclic rings and two stereogenic centres (C2 and C3 carbon atoms, Fig. 1). The reaction yields varied from moderate for NON and NON-Br (22–26%) to high for NON-CF₃ (82%). Garg et al.²¹ previously reported that lactols and hemiaminals behave as masked carbaldehydes under the conditions of a Fischer indole synthesis, resulting in the formation of various indoline derivatives with two heterocyclic rings and two stereogenic centres (Scheme 2, top). Therefore, we propose that the formation of the NON-R compounds occurs via an interrupted Fischer indolization^{22,23}. It's worth noting that the 1,3,5-oxadiazine moiety is a powerful heterocyclic framework with applications in pharmaceuticals, agriculture, and industry. This makes the facile synthesis of NON-R (R = H, CF₃ and Br) materials interesting in its own right^{24–28}.

All NON-compounds are white solids, stable in air and soluble in common polar organic solvents dichloromethane, acetone, THF and poorly soluble in hexane. The purity of the products was confirmed by ¹H, ¹³C and ¹⁹F NMR, High-Resolution Mass Spectrometry and X-ray diffraction analysis. The thermal stability of NON-materials increases from NON-Br (235 °C) to NON (256 °C) to NON-CF₃ (262 °C, Fig. S12). The central oxadiazine ring possesses two groups of distinctive proton resonances: the first as a doublet at

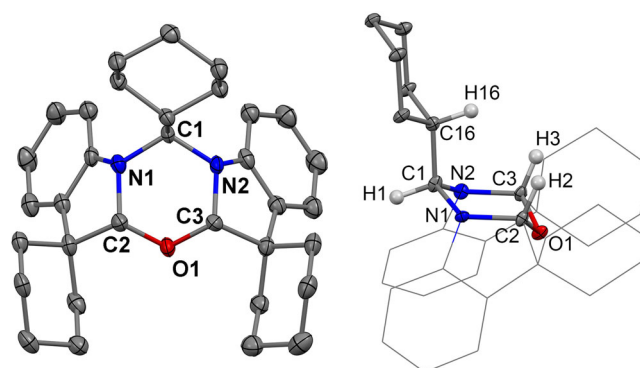


Fig. 1 | X-ray crystal structure of NON-compound. X-ray crystal structure of NON-compound front view (left, hydrogen atoms omitted for clarity) and side view (right, with selected hydrogen atoms). Ellipsoids are shown at the 50% level.

4.9 ppm for C1–H1, and the second is a singlet at 5.2 ppm for C2–H2 and C3–H3 (see Supplementary File). Crystals of NON-materials were grown by layering dichloromethane solutions with hexanes (Figs. 1, S8–S10). All three compounds possess *meso*-stereochemistry (R for C2 and S for C3). Similar stereochemical observations for the fused 1,3,5-oxadiazine rings have been reported by Ghinet et al.²⁴. The X-ray crystal structure revealed that the central oxadiazine six-membered ring adopts a chair-conformation where the H2 and H3 atoms occupy an axial position, whereas the H1 atom occupies an equatorial position (Fig. 1). Both indoline and spiro-cyclohexyl moieties of the NON-materials point in opposite directions with respect to the central

Table 1 | Cyclic voltammetry and additional photophysical parameters

	Oxidation			E_{HOMO}	E_{LUMO}	$E_{\text{opt-gap}}$	λ_{abs} (nm), ^b	S_1	T_1	$S_{\text{H/L}}$ ^d
	$E_{1\text{st}}$	$E_{\text{onset ox}}$	$E_{2\text{nd}}$	eV	eV ^a	eV	($\epsilon \times 10^3 \text{ M}^{-1} \text{ cm}^{-1}$)	eV ^c	eV ^c	
NON	+0.50	+0.37	–	–5.76	–1.90	3.86	264 (28), 294 (10.5), 304 (sh)	3.91	3.35	0.62
NON-CF ₃	+0.90 (100)	+0.75	+1.38	–6.14	–2.24	3.9	273 (21.2), 302 (sh)	4.36	3.31	0.66
NON-Br	+0.62 (90)	+0.51	+1.12	–5.90	–2.21	3.69	270 (15.7), 304 (4.1)	4.36	3.21	0.62

^aIn 1,2-difluorobenzene (DFB) solution, recorded using a glassy carbon electrode, concentration 1.4 mM, supporting electrolyte [nBu₄N][PF₆] (0.13 M), measured at 0.1 V s^{–1} while Ag wire was used as quasi-reference electrode. $E_{\text{HOMO}} = -(E_{\text{onset ox}} \text{ Fc/Fc}^+ + 5.39) \text{ eV}$; $E_{\text{LUMO}} = E_{\text{opt gap}} + E_{\text{HOMO}} \text{ eV}$, see Table S2 and Fig. S11.

^bConcentration $3.57 \times 10^{-5} \text{ M}$ for NON, $3.16 \times 10^{-5} \text{ M}$ for NON-CF₃; $2.69 \times 10^{-5} \text{ M}$ for NON-Br.

^c S_1 and T_1 energy levels based on the onset values of the emission spectra blue edge in MeTHF glasses at 77 K and 298 K.

^d $S_{\text{H/L}}$ is an overlap integral between HOMO and LUMO calculated by DFT.

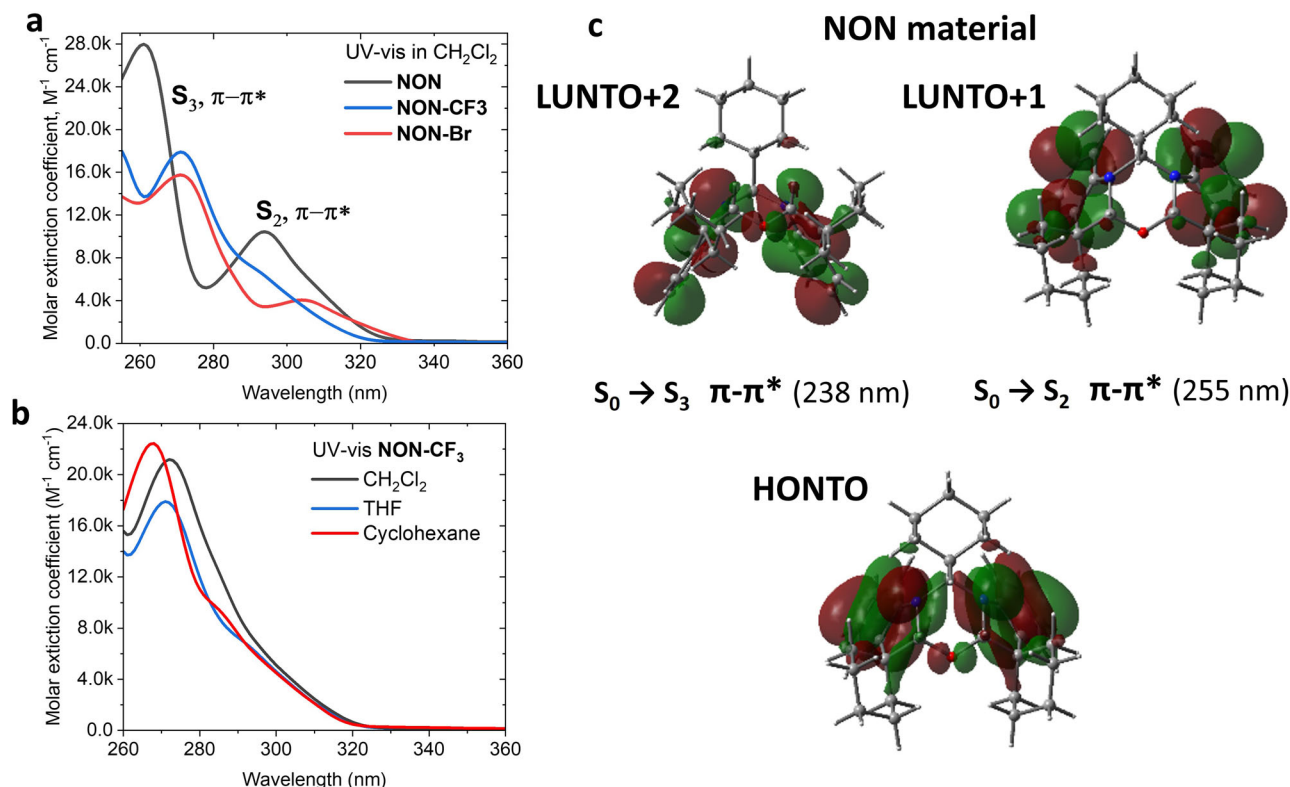


Fig. 2 | UV-vis absorption and frontier molecular orbitals distribution for NON-materials. UV-vis absorption for NON-materials in dichloromethane solution (a) and solvent of different polarity for NON-CF₃ (b); molecular orbitals distribution

involved in vertical excitations for NON-materials (c). There is ca 40 nm offset between the gas-phase calculated energy of the transition and observed UV-vis absorption in solution.

oxazine core, thus forming voids above and below the central ring, which are capable of accommodating solvent molecules (for instance, hexane, see Fig. S8). Molecules of the NON-materials form a three-dimensional network through weak C–H...π, C–H...F, C–H...Br or C–H^{δ+}(phenyl)...^δ⁺H–C(cyclohexyl) interactions between neighbouring molecules.

Cyclic voltammetry experiments were performed to investigate the redox properties of NON, NON-Br, and NON-CF₃ in 1,2-difluorobenzene solution (Fig. S11). The data is summarised in Table 2. The NON-compound exhibits non-reversible oxidation at a peak potential of $E_p = +0.5 \text{ V}$. The NON-CF₃ material shows two oxidation processes: the first one is reversible ($E_{1/2} = +0.90 \text{ V}$), while the second is irreversible with E_p at +1.38 V. The NON-Br compound shows two reversible oxidations at $E_{1/2} = +0.62$ and +1.12 V. The onset of the first oxidation potential (E_{onset}) values was used to calculate the energy level of the highest occupied molecular orbital (E_{HOMO} , see Table 1) for the NON-R materials. The E_{HOMO} energy correlates with the electron-withdrawing strength of the substituent R, i.e., it increases in line from –5.76 (R = H) to –5.90 (R = Br) and –6.14 eV (R = CF₃). The oxidation process of the NON-compounds is likely centred on the indoline moiety, which is supported

by the theoretical calculations which predict the localization of the HOMO to this region (see Fig. 3c, Table S4). The reduction potential for all three compounds was beyond the solvent discharge potential, therefore, a direct calculation of the LUMO energy level is impossible. Instead, the E_{LUMO} energy was estimated indirectly using the equation $E_{\text{LUMO}} = E_{\text{opt-gap}} + E_{\text{HOMO}}$, where $E_{\text{opt-gap}}$ is taken as the red-onset of the lowest energy absorption band in the UV-vis absorption spectra in a dichloromethane solution (*vide infra*, Table 1).

Photophysical properties

To investigate photophysical properties, UV-visible absorption (Fig. 2) and photoluminescence (Fig. 3) spectra were recorded for all NON-compounds. The data is summarized in Tables 1 and 2. All compounds show a strong absorption band in the range 260–280 nm (extinction coefficient ϵ up to $2.8 \times 10^4 \text{ M}^{-1} \text{ cm}^{-1}$, Table S3) and a low-energy absorption band at ca. 304 nm with ϵ coefficient up to $4 \times 10^3 \text{ M}^{-1} \text{ cm}^{-1}$ (Table S3). Theoretical calculations revealed that oscillator strength coefficients (f) for S₀→S₁ (HOMO→LUMO) are nearly zero for all NON-materials. Further analysis of the TD-DFT results (Fig. 2), for instance for the NON-compound,

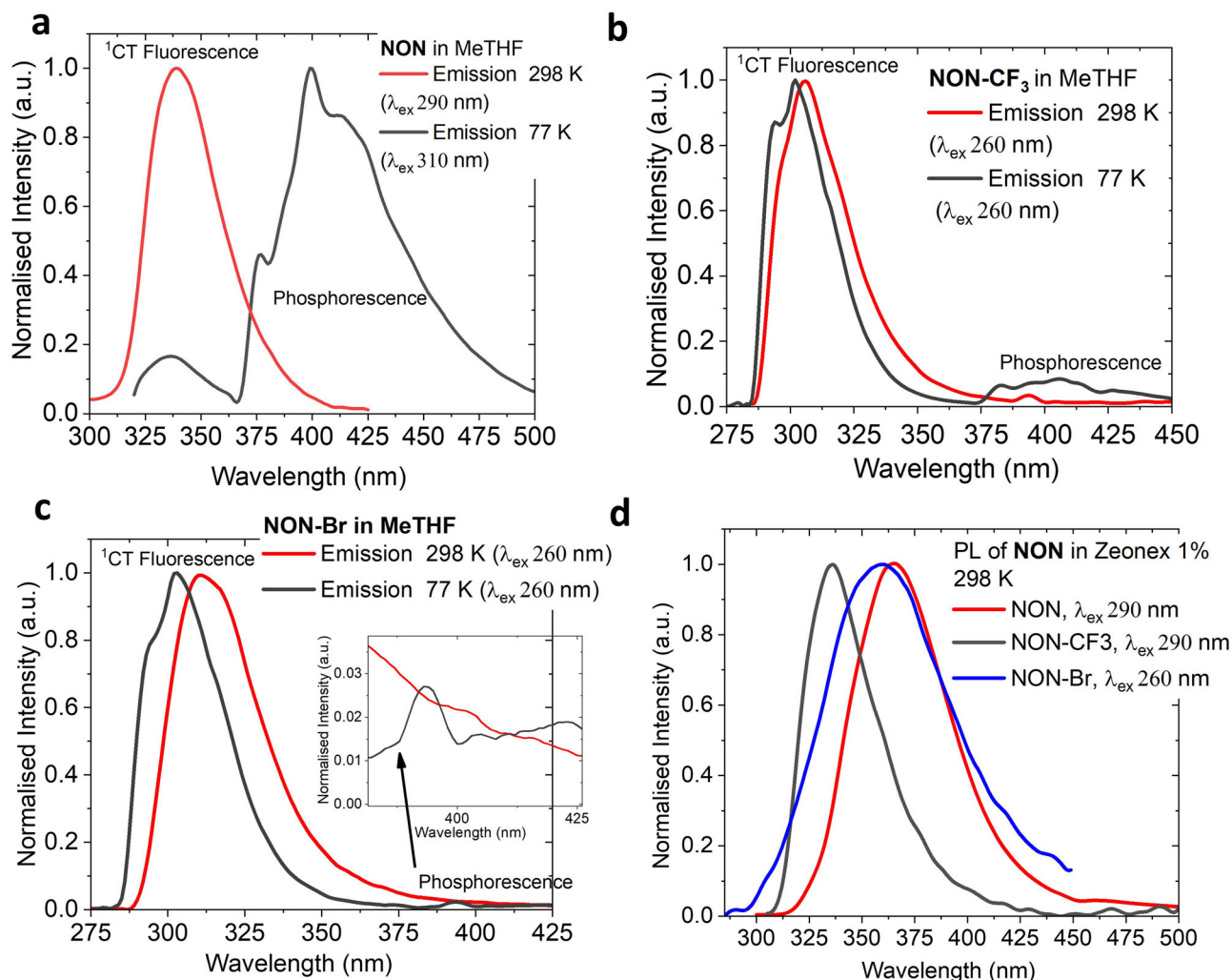


Fig. 3 | Photoluminescence spectra for NON-materials. Photoluminescence (PL) spectra for compounds NON (a), NON- CF_3 (b) and NON-Br (c) in MeTHF solution (at 298 K and frozen glass at 77 K); PL for NON-compounds in 1% by weight Zeonex matrix at 298 K (d).

Table 2 | Photophysical properties of the NON-materials in MeTHF solution and 1% Zeonex matrix at 298 and 77 K

	298 K			k_r (10^8 s^{-1}) ^b	k_{nr} (10^8 s^{-1}) ^c	77 K	
	λ_{max} (nm)	τ (ns)	Φ (%), N_2) ^a			λ_{max} (nm)	τ
MeTHF solution							
NON	338	1.4	23	1.7	5.5	337 400	2.6 ns >3 s
NON-CF ₃	310	0.9 ^d	12	1.4	10	302 400	5.9 ns >3 s
NON-Br	315	1.1 ^d	–	–	–	302 393	– >3 s
1% Zeonex matrix							
NON	336	1.8	21	1.2	4.4	–	–
NON-CF ₃	306	0.9 ^d	10	1.2	10	–	–
NON-Br	350	1.1 ^d	3	0.27	8.7	–	–

^aQuantum yields determined using an integrating sphere.

^bRadiative constant $k_r = \Phi/\tau$.

^cnonradiative constant $k_{nr} = (1 - \Phi)/\tau$.

^dIn case of two-component lifetime τ an average was used: $\tau_{\text{av}} = (B_1/(B_1 + B_2))\tau_1 + (B_2/(B_1 + B_2))\tau_2$, where B_1 and B_2 are the relative amplitudes for τ_1 and τ_2 , respectively.

revealed the intense vertical excitation: $S_0 \rightarrow S_2$ ($f=0.08$; HOMO \rightarrow LUMO + 1) and $S_0 \rightarrow S_3$ ($f=0.17$; HOMO \rightarrow LUMO + 2) which are all ascribed to $\pi-\pi^*$ transitions within the indolines of the NON-materials (Tables S4, S6 and S7). The optical gap ($E_{\text{opt-gap}}$) values for all NON-

materials were calculated from the red-onset of the lowest energy absorption band: 3.72 eV for NON, 3.86 eV for NON-Br and 3.90 eV for NON- CF_3 . All absorption bands demonstrate very little solvatochromic effect, as shown in Fig. 2b for the compound NON- CF_3 (see Supporting Files, Figs. S13–S15 for

all compounds). This indicates only a minor change in the dipole moment upon vertical excitation from the ground S_0 to excited S_1 states and is reflected in the TD-DFT theoretical calculations (Table S5).

All NON-compounds exhibit featureless and narrow near-UV-fluorescence with a full width at half maximum (FWHM) of 3400 cm^{-1} (40 nm) in MeTHF solution or Zeonex films at 295 K (Figs. 3 red line, S16–S21). The electron-withdrawing substituents on the indoline moieties lead to a blue shift in emission from 338 nm for NON to 310 and 315 nm for NON- CF_3 and NON-Br, respectively. This observation is corroborated by theoretical calculations that show the HOMO is localised over the indoline moieties. Therefore, increasing the electron-withdrawing strength of the substituents attached to the indoline moiety results in the stabilization of the HOMO energy level and an increase in the emission energy. The photoluminescence quantum yields (PLQY) for UV-luminescence increase from NON-Br (3%) to NON- CF_3 (12%) to NON (23%) in the MeTHF solution at 295 K.

All NON-materials, in all media, exhibit an excited state lifetime on the nanosecond time scale in the range of 0.9–1.8 ns, which is typical for the fluorescence emission mechanism. Figure 3 depicts the emission profiles of the NON-compounds in frozen MeTHF glasses at 77 K (black line, Table 2). The emission spectra of NON at 77 K is dominated by a deep-blue and vibronically resolved phosphorescence, peaking at 400 nm. The excited state lifetime is too long to be measured by a gated Xenon flashlamp. However, the emission was observed with the naked eye to persist for more than 3 s after the excitation ceased. Unlike NON, the emission spectra of NON- CF_3 and NON-Br compounds are dominated by UV-fluorescence (306–337 nm), with a minor contribution from the deep-blue phosphorescence component at 77 K (Fig. 3b, c). Similar to NON, the excited state lifetime of the phosphorescence is longer than 3 s, while the fluorescence excited state lifetime only slightly increases up to 5.9 ns upon cooling.

The energy levels of the singlet (S_1) and triplet (T_1) excited states for all NON-materials were deduced from the blue-onsets of the fluorescent and phosphorescent profiles (Figs. 3, S23, Table 1) at 77 K. The NON and NON- CF_3 materials exhibit a high triplet energy level at 3.3 eV, which is higher than the most popular host material DPEPO (3.0 eV) and on par with the most stable deep-blue OLED host material – PPBi (3.3 eV). The computed values align well with the experimental results (Table S6). The theoretical calculations show that both frontier orbitals, HOMO and LUMO, are primarily localized over the indoline rings of the NON-compounds (Table S4), resulting in a large frontier orbital overlap integral (0.62–0.66) for all NON-materials (Table S4). This is largely due to the absence of spatially separated donor and acceptor moieties, which results in a significant stabilization of the T_1 energy level and an energy difference with the singlet excited state, ΔE_{ST} , up to 1.15 eV. Note that the central oxadiazine core with spiro- sp^3 carbon atoms acts as an insulator, preventing extended conjugation between two indoline moieties for the NON-materials, which prevents further lowering of the T_1 energy level. It has previously been demonstrated that small molecule hosts^{29,30} show triplet energy variance depending on the degree of conjugation and magnitude of the dihedral angle between the cycles involved, for instance, carbazole moieties in CBP ($T_1 = 2.64\text{ eV}$), mCBP ($T_1 = 2.84\text{ eV}$), oCBP ($T_1 = 3.0\text{ eV}$, Scheme 1)²⁹ and others^{29,30}. Therefore, the novelty of NON-host molecular design strongly benefits from the bulky cyclohexyl moieties, absence of any inter-cycle bonds and spiro- sp^3 carbon atom breaking the conjugation thus explaining the high triplet energy level and making NON-hosts more robust towards the local environment.

Device fabrication, characterisation, and performance

We assessed all NON-materials against the criteria outlined in the introduction to identify a promising host material for the development of deep-blue OLED devices. The NON- CF_3 material exhibits good thermal stability, a wide energy gap (3.9 eV) thanks to a well-stabilised HOMO (−6.1 eV) and a destabilised LUMO (−2.2 eV), a high triplet energy level of 3.3 eV, and excellent volatility during the sublimation process due to three cyclohexyl groups. These attributes motivated us to test the NON- CF_3 material as a host with our recently developed Carbene-Metal-Amide (CMA) TADF material P170 (Fig. 4a)³¹. First two triplet states of complex P170 are T_1 (^3CT 2.77 eV) and T_2 (^3LE

3.29 eV)³¹ are lower in energy compared to the first triplet state of the NON- CF_3 host (T_1 is 3.3 eV) thus preventing the Dexter energy transfer back to the host material. OLED devices were fabricated via thermal vapour deposition. The device architecture is shown in Fig. 4, along with the chemical structures of the materials used. The 30 nm layer of 1,1-bis[4-[N,N-di(4-toyl)amino]phenyl]cyclohexane (TAPC) and a 10 nm layer of 9,9'-biphenyl-2,2'-diylbis-9H-carbazole (oCBP) function as hole transport layers. In each device, the 20 nm thick emissive layer (EML) consists of an emitting material doped at 10% by weight into the NON- CF_3 host. A 45 nm layer of diphenyl-4-triphenylsilyl-phenylphosphine oxide (TSPO1) is used for electron transport. Four EML compositions were prepared using four different host materials, namely PPBi, TCP, mCP and NON- CF_3 (Fig. 4a), to evaluate and compare the performance of NON- CF_3 .

The electroluminescence spectra for devices at 6 V are shown in Fig. 4, and a summary of the performance data for each device is given in Table 3. The use of NON- CF_3 as a host material results in a blue shift of up to 31 nm for the electroluminescence from P170 compared to the other host materials tested. This leads to a highly desirable 448 nm EL from P170 with a narrow FWHM of ca. 60 nm in a NON- CF_3 host. This result is favourable when comparing NON- CF_3 to the DPEPO host, where the deep-blue OLED (EML: P170 10% in DPEPO) demonstrated a 30 nm wider FWHM value (ca. 90 nm)³¹. Therefore, a commonly cited disadvantage of organometallic TADF materials, such as their broad EL emission profiles associated with the emission occurring from a charge transfer (CT) state, could be circumvented by using the NON- CF_3 host material. This enables narrow EL profiles and better CIE-colour coordinates. The phenomena of the PL^{31–34} and EL^{31,35} blue shift of the CT emission for CMA materials were studied in detail and explained by thermally activated diffusion and electrostatic interactions between CMA emitter with host molecules.

Devices utilizing NON- CF_3 exhibit an increased turn-on voltage, which is reported as the applied bias for luminescence to equal 1 cd m^{-2} . This suggests a higher barrier for charge injection into the emitting layer. Figure 4 shows the current density–voltage–luminescence (J–V–L) curves for each OLED device. Devices experience luminescence roll-off when operating above 11 V, indicating a need for further improvement in the molecular design of the NON-host materials. However, the OLED devices hosted by NON- CF_3 achieved an External Quantum Efficiency EQE_{max} value of 21.0%, the highest value among all tested host materials. Impressively, OLED devices containing P170 doped into NON- CF_3 were operational at 100 cd m^{-2} with an EQE of 9.2%, which is comparable to commercially available host materials such as TCP and mCP tested in this work. The EQE performance is likely associated with higher PLQY values for P170 films in the NON- CF_3 host (82%) compared to TCP films (38%). These findings suggest a high potential for NON-host materials to be used as host materials for deep-blue OLEDs.

Conclusion

We discovered an unexpected product of the interrupted Fischer indolization reaction which has enabled a straightforward synthesis of optionally substituted 1,3,5-oxadiazines (NON) in good yields. Our protocol involves a single-step condensation reaction between cost-effective substituted hydrazines and carbaldehydes to prepare NON-compounds with good thermal stability up to 262.5°C . We demonstrated that all NON-materials emit only fast UV-fluorescence (310–338 nm) at room temperature, while a long-lived (over 3 s) deep-blue phosphorescence emerges upon cooling to 77 K. Our theoretical calculations revealed large frontier orbitals overlap integral values up to 0.66 for the NON-materials which is rationalised by the significant energy difference between singlet (S_1) and triplet (T_1) excited states up to 1.15 eV.

Our photophysical and electrochemical investigation into the new 1,3,5-oxadiazine materials revealed their suitability, from an energy level standpoint, for use as host materials in OLED devices. NON- CF_3 was selected for use in proof-of-concept devices based on its good thermal stability, wide energy gap (3.9 eV), well-stabilised HOMO (−6.1 eV) and destabilised LUMO (−2.2 eV), high triplet energy level (3.3 eV), and excellent volatility, thanks to the bulky cyclohexyl groups that prevent strong intermolecular contacts. Given the novel molecular design of NONs and their remarkably

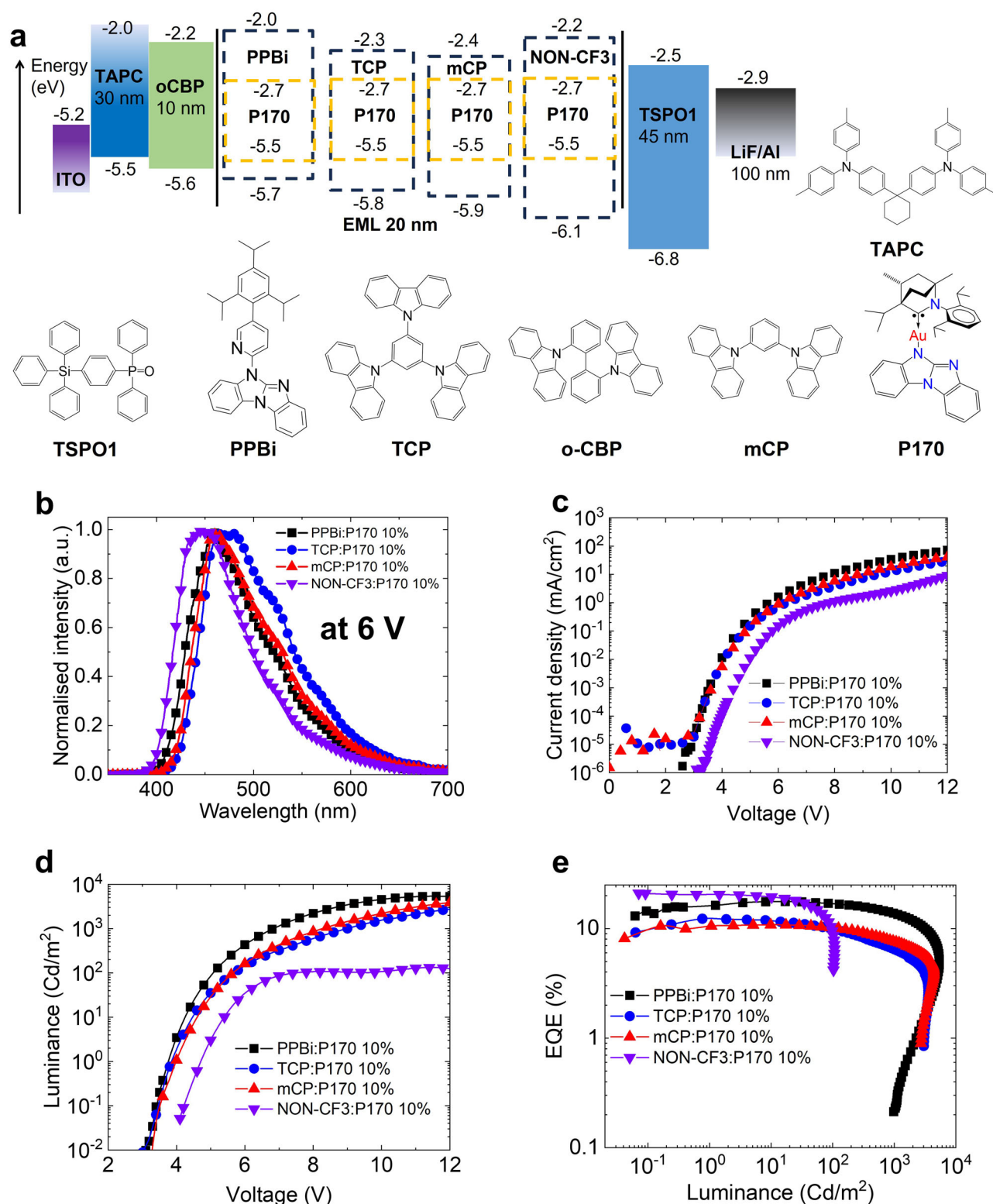


Fig. 4 | Vapour-deposited OLED device architectures. **a** OLED architecture for P170 doped into different hosts at 10% by weight and chemical formulae of materials used in the devices; **b** Normalised electroluminescence spectra from devices

incorporating P170 10% by weight in host-guest structures; **c** current density-voltage plot; **d** luminance-voltage plot; **e** EQE versus luminance plot.

simple synthesis, we are impressed that OLED devices using a CMA TADF emitter and NON-CF₃ host achieved EQE values up to 21%. Furthermore, we demonstrated how the use of a NON-host material can facilitate excellent deep-blue colour emission by producing a blue-shifted and narrow (60 nm) electroluminescence profile in comparison to conventional host materials.

This work introduces a new class of OLED host materials. Further modifications to the host material structure can be made by decorating with electron donating or withdrawing groups to enhance hole and electron transport mobility and pave the way to high-performance and stable deep-blue OLEDs.

Table 3 | Performance data of evaporated OLEDs

OLED	Host	V _{on} ^a (V)	EQE _{Max} (%)	EQE ₁₀₀ ^b (%)	λ _{max} (nm)	CIE (x;y)
Au1	1 PPBi	3.4	17.7	16.9	457	0.18; 0.23
	2 TCP	3.5	12.3	9.9	479	0.20; 0.30
	3 mCP	3.5	10.8	10.2	461	0.19; 0.26
	4 NON-CF ₃	4.2	21.0	9.2	448	0.17; 0.16

^aV_{on} at 0.1 cd m⁻².^bEQE at 100 cd m⁻².

Methods

Material preparation

The Au1 complex P170 was obtained according to the literature. All NON-materials were purified on a silica gel column, recrystallised from hexane, while NON-CF₃ was sublimed to have high purity for OLED fabrication (See Supplementary Methods).

Photophysical properties

Solution UV-visible absorption spectra were recorded on a Cary 500 UV-vis-NIR spectrometer for a wavelength range 250–700 nm. Photoluminescence measurements were recorded using an Edinburgh Instruments FLS920 spectrometer. All excited state lifetimes were measured on FLS920 spectrometer with mono- and biexponential fitting provided by Edinburgh Instruments Fluoracore software v2.6.1. Absolute photoluminescent quantum yields were measured directly with a Quantaurus-QY Absolute PL quantum yield spectrometer.

Computational details

The ground and excited states of all complexes were studied by DFT and TD-DFT³⁶ respectively, using Tamm-Dancoff approximation³⁷. All calculations were carried out by Gaussian 16³⁸, employing the global hybrid MN15 functional³⁹ and the def2-TZVP basis set⁴⁰. The overlap integrals between HOMO and LUMO were calculated using the Multiwfn program⁴¹.

OLED fabrication and characterisation

OLED devices were fabricated by high-vacuum (10⁻⁷ Torr) thermal evaporation on ITO-coated glass substrates with sheet resistance of 15 Ω/□. Substrates were cleaned by sonication in a non-ionic detergent, deionised water, acetone, and isopropyl alcohol and subject to an oxygen plasma treatment for 10 min. Layers were deposited at rates of 0.1–2 Å s⁻¹. TCP, PPBi and mCP were purchased from Luminescence Technology Corp. TPBi, DPEPO and TSPO1 were purchased from Shine Materials. All purchased materials were used as received. OLED current density-voltage measurements were made using a Keithley 2400 source-meter unit. The luminance was measured on-axis using a 1 cm² calibrated silicon photodiode at a distance of 15 cm from the front face of the OLED. Electroluminescence spectra were measured using a calibrated OceanOptics Flame spectrometer. Lifetime measurements were measured with a Keithley 2400 source-meter unit and a 0.75 cm² silicon photodiode. The devices were held under rough vacuum (~10⁻³ Torr).

Data availability

Supplementary data are available in the online version of the paper. This includes Supplementary data 1, which includes the crystallographic data for this paper. The X-ray crystallographic coordinates for structures reported in this Article have been deposited at the Cambridge Crystallographic Data Centre (CCDC), under deposition number CCDC 2363678 for NON; 2363679 for NON-CF₃; 2363680 for NON-Br. These data can be obtained free of charge from The Cambridge Crystallographic Data Centre via www.ccdc.cam.ac.uk/data_request/cif. Authors can confirm that all relevant data are included in the paper and/ or its supplementary information files.

Received: 9 July 2024; Accepted: 25 November 2024;

Published online: 19 December 2024

References

1. Tang, C. W. & Vanslyke, S. A. Organic electroluminescent diodes. *Appl. Phys. Lett.* **51**, 913–915 (1987).
2. Jeong, E. G., Kwon, J. H., Kang, K. S., Jeong, S. Y. & Choi, K. C. A review of highly reliable flexible encapsulation technologies towards rollable and foldable OLEDs. *J. Inf. Disp.* **21**, 19–32 (2020).
3. Baldo, M. A., O'Brien, D. F., Thompson, M. E. & Forrest, S. R. Excitonic singlet-triplet ratio in a semiconducting organic thin film. *Phys. Rev. B* **60**, 14422 (1999).
4. Fan, X. et al. Enhancing reverse intersystem crossing via secondary acceptors: toward sky-blue fluorescent diodes with 10-fold improved external quantum efficiency. *ACS Appl. Mater. Interfaces* **11**, 4185–4192 (2019).
5. Endo, A. et al. Efficient up-conversion of triplet excitons into a singlet state and its application for organic light emitting diodes. *Appl. Phys. Lett.* **98**, 083302 (2011).
6. Baldo, M. A. et al. Highly efficient phosphorescent emission from organic electroluminescent devices. *Nature* **395**, 151–154 (1998).
7. Adachi, C., Baldo, M. A., Thompson, M. E. & Forrest, S. R. Nearly 100% internal phosphorescence efficiency in an organic light emitting device. *J. Appl. Phys.* **90**, 5048–5051 (2001).
8. Tao, Y. et al. Thermally activated delayed fluorescence materials towards the breakthrough of organoelectronics. *Adv. Mater.* **26**, 7931–7958 (2014).
9. Shi, Y.-Z. et al. Recent progress in thermally activated delayed fluorescence emitters for nondoped organic light-emitting diodes. <https://doi.org/10.1039/d1sc07180g> (2022).
10. Zhang, T. et al. Highly twisted thermally activated delayed fluorescence (TADF) molecules and their applications in organic light-emitting diodes (OLEDs). *Angew. Chem. Int. Ed.* **62**, e202301896 (2023).
11. Cai, X., Su, S.-J., Cai, X. Y. & Su, S.-J. Marching toward highly efficient, pure-blue, and stable thermally activated delayed fluorescent organic light-emitting diodes. *Adv. Funct. Mater.* **28**, 1802558 (2018).
12. Giebink, N. C. et al. Intrinsic luminance loss in phosphorescent small-molecule organic light emitting devices due to bimolecular annihilation reactions. *J. Appl. Phys.* **103**, 044509 (2008).
13. Wong, M. Y. & Zysman-Colman, E. Purely organic thermally activated delayed fluorescence materials for organic light-emitting diodes. *Adv. Mater.* **29**, 1605444 (2017).
14. Choi, S. et al. Optimized structure of silane-core containing host materials for highly efficient blue TADF OLEDs. *J. Mater. Chem. C. Mater.* **5**, 6570–6577 (2017).
15. Yeon Kwon, N. et al. Rational molecular design strategy for host materials in thermally activated delayed fluorescence-OLEDs suitable for solution processing. *ACS Appl. Mater. Interfaces* **15**, 28277–28287 (2023).
16. Oner, S. & Bryce, M. R. A review of fused-ring carbazole derivatives as emitter and/or host materials in organic light emitting diode (OLED) applications. *Mater. Chem. Front.* **7**, 4304 (2023).
17. Brigaud, T. et al. High triplet energy host materials for blue TADF OLEDs—a tool box approach. *Front. Chem.* **1**, 657 (2020).
18. Chatterjee, T. & Wong, K. T. Perspective on host materials for thermally activated delayed fluorescence organic light emitting diodes. *Adv. Opt. Mater.* **7**, 1800565 (2019).
19. Zhang, J., Ding, D., Wei, Y. & Xu, H. Extremely condensing triplet states of DPEPO-type hosts through constitutional isomerization for high-efficiency deep-blue thermally activated delayed fluorescence diodes. *Chem. Sci.* **7**, 2870 (2016).
20. Ahn, D. H. et al. Highly twisted donor-acceptor boron emitter and high triplet host material for highly efficient blue thermally activated delayed fluorescent device. *ACS Appl. Mater. Interfaces* **11**, 14909 (2019).
21. Boal, B. W., Schammel, A. W. & Garg, N. K. An interrupted fischer indolization approach toward fused indoline-containing natural products. *Org. Lett.* **11**, 3458 (2009).

22. Schammel, A. W., Boal, B. W., Zu, L., Mesganaw, T. & Garg, N. K. Exploration of the interrupted Fischer indolization reaction. *Tetrahedron* **66**, 4687–4695 (2010).
23. Yang, Z. et al. Recent advances in organic thermally activated delayed fluorescence materials. *Chem. Soc. Rev.* **46**, 915 (2017).
24. Ghinet, A. et al. 1,3,5-oxadiazine framework by oxygen vs. nitrogen trapping of an N-acyliminium ion derived from N,O-bis-TMS pyroglutamic acid. *ChemistrySelect* **2**, 10654–10660 (2017).
25. Strelnikova, J. O., Rostovskii, N. V., Khoroshilova, O. V., Khlebnikov, A. F. & Novikov, M. S. An efficient synthesis of functionalized 2H-1,3,5-oxadiazines via metal-carbenoid-induced 1,2,4-oxadiazole ring cleavage. *Synthesis* **53**, 348–358 (2021).
26. Li, C. C., Zhong, Y. Y. & Xu, L. Z. Rac-(E)-3-[1-(2-Chlorophenyl)ethyl]-5-methyl-N-nitro-1,3, 5-oxadiazinan-4-imine. *Acta Crystallogr. Sect. E Struct. Rep. Online* **66**, o2456–o2456 (2010).
27. Maiefisch, P. et al. Chemistry and biology of thiamethoxam: a second generation neonicotinoid. *Pest Manag. Sci.* **57**, 906–913 (2001).
28. Heravi, M. M., Rohani, S., Zadsirjan, V. & Zahedi, N. Fischer indole synthesis applied to the total synthesis of natural products. *RSC Adv.* **7**, 52852–52887 (2017).
29. Gong, S. et al. Simple CBP isomers with high triplet energies for highly efficient blue electrophosphorescence. *J. Mater. Chem.* **22**, 2894–2899 (2012).
30. Wright, I. A. et al. Conformational dependence of triplet energies in rotationally hindered N- and S-heterocyclic dimers: new design and measurement rules for high triplet energy OLED host materials. *Chem. Eur. J.* **27**, 6545–6556 (2021).
31. Brannan, A. C. et al. Deep-blue and fast delayed fluorescence from carbene-metal-amides for highly efficient and stable organic light-emitting diodes. *Adv. Mater.* **36**, 2404357 (2024).
32. Feng, J. et al. Environmental control of triplet emission in donor-bridge-acceptor organometallics. *Adv. Funct. Mater.* **30**, 1908715 (2020).
33. Föller, J. & Marian, C. M. Rotationally assisted spin-state inversion in carbene-metal-amides is an artifact. *J. Phys. Chem. Lett.* **8**, 5643–5647 (2017).
34. Conaghan, P. J. et al. Highly efficient blue organic light-emitting diodes based on carbene-metal-amides. *Nat. Commun.* **11**, 1758 (2020).
35. Weigend, F. & Ahlrichs, R. Balanced basis sets of split valence, triple zeta valence and quadruple zeta valence quality for H to Rn: design and assessment of accuracy. *Phys. Chem. Chem. Phys.* **7**, 3297–3305 (2005).
36. Furche, F. & Rappoport, D. Density functional methods for excited states: equilibrium structure and electronic spectra. In *Computational Photochemistry*, Vol. 16 (ed. Olivucci, M.) 93–128 (Elsevier, Amsterdam, The Netherlands, 2005).
37. Hirata, S. & Head-Gordon, M. Time-dependent density functional theory within the Tamm–Dancoff approximation. *Chem. Phys. Lett.* **314**, 291–299 (1999).
38. Frisch, M. J. et al. *Gaussian 16; Revision A. 03* (Gaussian Inc., Wallingford, CT, USA, 2016).
39. Yu, H. S., He, X., Li, S. L. & Truhlar, D. G. MN15: a Kohn–Sham global-hybrid exchange–correlation density functional with broad accuracy for multi-reference and single-reference systems and noncovalent interactions. *Chem. Sci.* **7**, 5032–5051 (2016).
40. Weigend, F., Häser, M., Patzelt, H. & Ahlrichs, R. RI-MP2: optimized auxiliary basis sets and demonstration of efficiency. *Chem. Phys. Lett.* **294**, 143–152 (1998).
41. Lu, T. & Chen, F. Multiwfn: a multifunctional wavefunction analyzer. *J. Comput. Chem.* **33**, 580–592 (2012).
42. Sun, D. et al. Arylsilanes and siloxanes as optoelectronic materials for organic light-emitting diodes (OLEDs). *J. Mater. Chem. C* **3**, 9496 (2015).
43. Zyryanov, G. V., Kovalev, I. S., Egorov, I. N., Rusinov, V. L. & Chupakhin, O. N. Synthesis of symmetrical dicarbazole-biphenyls,

components of phosphorescent organic light-emitting diodes (PHOLEDs) using organocuprates. *Chem. Heterocycl. Comp.* **47**, 571–574 (2011). Translated from *Khimiya Geterotsiklicheskikh Soedinenii* **5**, 692–695 (2011).

Acknowledgements

A.S.R. acknowledges the support from the Royal Society (grant nos. URF\R1\180288, RGF\EA\181008, URF\R\231014), EPSRC (grant code EP/K039547/1). M.L. acknowledges the Academy of Finland Flagship Programme, Photonics Research and Innovation (PREIN), decision 320166, and the Finnish Grid and Cloud Infrastructure resources (urn:nbn:fi:research-infras-2016072533). N.L.P. acknowledges the Doctoral Programme in Science, Forestry and Technology (Lumeto, University of Eastern Finland). European Union's Horizon 2020 research and innovation programme grant agreement no. 101020167 (H.-H.C.). We thank Dr Louise Natrajan, EPSRC and the University of Manchester for access the Centre for Radiochemistry Research National Nuclear User's Facility (NNUF, EP/T011289/1) to use the FLS-1000 fluorometer.

Author contributions

C.R. performed the synthesis, steady-state photoluminescence and electrochemistry studies. H.-H.C. developed and characterized the OLED devices. A.S.R. performed X-ray crystallography. A.C.B. performed the synthesis of the **P170** complex. N.L.P. and M.L. carried out theoretical calculations. N.G. and A.S.R. planned the project and designed the experiments. C.R. and A.S.R. co-wrote the manuscript. All authors contributed to the discussion of the results, and analysis of the data and reviewed the manuscript.

Competing interests

The authors declare no competing interests.

Additional information

Supplementary information The online version contains supplementary material available at <https://doi.org/10.1038/s42004-024-01377-y>.

Correspondence and requests for materials should be addressed to Mikko Linnolahti, Neil C. Greenham or Alexander S. Romanov.

Peer review information *Communications Chemistry* thanks the anonymous reviewers for their contribution to the peer review of this work. Peer review reports are available.

Reprints and permissions information is available at <http://www.nature.com/reprints>

Publisher's note Springer Nature remains neutral with regard to jurisdictional claims in published maps and institutional affiliations.

Open Access This article is licensed under a Creative Commons Attribution 4.0 International License, which permits use, sharing, adaptation, distribution and reproduction in any medium or format, as long as you give appropriate credit to the original author(s) and the source, provide a link to the Creative Commons licence, and indicate if changes were made. The images or other third party material in this article are included in the article's Creative Commons licence, unless indicated otherwise in a credit line to the material. If material is not included in the article's Creative Commons licence and your intended use is not permitted by statutory regulation or exceeds the permitted use, you will need to obtain permission directly from the copyright holder. To view a copy of this licence, visit <http://creativecommons.org/licenses/by/4.0/>.

© The Author(s) 2024